universe

MDPI

Article

Upper Limit on the Diffuse Radio Background from GZK Photon Observation

Graciela B. Gelmini [1], Oleg Kalashev [2,3] and Dmitri Semikoz [4,*]

[1] Department of Physics and Astronomy, University of California Los Angeles, Los Angeles, CA 90095-1547, USA
[2] Institute for Nuclear Research of the Russian Academy of Sciences, 117312 Moscow, Russia
[3] Department of Physics, Novosibirsk State University, Pirogova 2, 630090 Novosibirsk, Russia
[4] Astroparticle Physics and Cosmology, Universitè Paris Citè, CNRS/IN2P3, 75013 Paris, France
* Correspondence: semikoz@apc.in2p3.fr

Abstract: Here, we point out that an observation of ultrahigh energy cosmic ray (UHECR) photons, "GZK photons", could provide an upper limit on the level of the extragalactic radio background, depending on the level of UHECR proton primaries (to be determined after a few years of data taking by the Pierre Auger Observatory upgrade AugerPrime). We also update our 2005 prediction of the range of GZK photon fluxes expected from proton primaries.

Keywords: GZK photons; UHECR; diffuse radio background

check for updates

Citation: Gelmini, G.B.; Kalashev, O.; Semikoz, D. Upper Limit on the Diffuse Radio Background from GZK Photon Observation. *Universe* **2022**, *8*, 402. https://doi.org/10.3390/universe8080402

Academic Editor: Gabor David

Received: 2 June 2022
Accepted: 22 July 2022
Published: 31 July 2022

1. Introduction

The level of the extragalactic radio background (EGRB) has become a point of considerable interest in recent years. The Absolute Radiometer for Cosmology, Astrophysics and Diffuse Emission (ARCADE-2) balloonborne bolometer detected in 2009 [1] an excess over the cosmic microwave background radiation (CMB) at high radio frequencies, 3 to 90 GHz, after subtraction of the CMB and a model of Milky Way emission of more than double what is expected from known extragalactic point sources. Measurements from the Long Wavelength Array at 40 to 80 MHz and others [2] agree with the high ARCADE 2 level.

An overview of the state of the subject as of 2018 [3] showed that if the background seen by ARCADE-2 and other low-frequency experiments is extragalactic, its origin is an important open question in astrophysics, since its sources would have to be faint and much more numerous than known galaxies. The sources would need to be nonthermal due to the spectral index of the background. The detected excess was found to be an isotropic component with an antenna temperature as function of the frequency with a power law spectrum of index -2.58, flatter than known radio sources.

Several exotic extragalactic mechanisms have also been studied to explain the excess such as annihilating axionlike dark matter [4] or dark photons [5], supernova explosion of Population III stars [6], superconducting cosmic strings [7], radiative decay of relic neutrinos to sterile neutrinos [8], thermal emission from quark nugget dark matter [9], and accreting astrophysical black holes [10,11] or primordial black holes [12]. A local origin of the mentioned background in the Local Bubble, a low-density cavity in the interstellar medium around the Solar system, has been proposed as an alternative [13].

Understanding if the mentioned radio background is of extragalactic or local origin is essential to study the expected signature in the 60 to 80 MHz range associated with the 21 cm spin-flip transition of HI from the epoch of reionization. This is where EDGES (the Experiment to Detect the Global Epoch of Reionization Signature) [14] has found an absorption feature in 2018. Even a radio background with intensity 0.01 of the ARCADE-2 [1] result would have an observable effect at high-redshift 21 cm observations [6,15].

Here, we explore the possibility of obtaining an upper limit on the EGRB if photons are detected in ultrahigh energy cosmic rays (UHECRs) given a measured fraction of proton primaries in UHECRs. The origin of UHECRs, the cosmic rays with energies above 10^{18} eV, is a longstanding puzzle in astrophysics (for a recent review, see, e.g., [16]). In particular, the composition (namely, the fraction of primary protons and other nuclei) of the cosmic rays with energies beyond the Greisen–Zatsepin–Kuzmin (GZK) feature [17,18] at 4×10^{19} eV has still large uncertainties (see e.g., [19,20] and references therein). UHECRs are only observed through extensive air showers that they produce in the atmosphere, which makes determining the nature of their primary particles subject to the uncertainties of hadronic interaction models. The existing measurements have large errors and may contain unknown systematic effects. At EeV energies, Pierre Auger Observatory (Auger) and the Telescope Array (TA), find a predominantly light composition with a large fraction of primary protons. Above 2 EeV, Auger favors a mixed composition with mean mass steadily growing, while TA data seems to be in tension with this result, favoring a lighter composition [21]. However, Auger and TA data are compatible within the current statistical and systematic uncertainties. At energies above the GZK suppression, the total number of detected events is relatively small; thus, the composition is even more uncertain (see, e.g., [20,22,23]).

The results of Auger and TA indicate that UHECR primaries consist mostly of protons and heavier atomic nuclei, but there could be also primary photons. Photons and neutrinos are produced by interactions of ultrahigh energy charged particles with the background medium, either at the source site or during the propagation. Both Auger (since 2007 [24]) and TA have searched for UHECR photon primaries and obtained upper limits on their flux [20,25–27]. UHECR photons would be preferentially produced by proton photoproduction of pions on the microwave background, in the decay of π^0, the process that leads to the GZK effect. These are "GZK photons" [28–30]. The observed flux suppression at 4×10^{19} eV could also be due to photon disintegration of heavy nuclei or a limit in the maximum particle energy reached at the sources, in which case many less ultrahigh-energy photons would be produced (e.g., considering only Fe primaries reduces the level of photons by more than an order of magnitude, see, e.g., Figure 7 of [27]). The reason is that UHECR nuclei of atomic number A and energy E disintegrating at the GZK threshold produce protons, neutrons, and lighter nuclei of energies $\simeq E/A$, which generally are below the photo-pion production threshold. Since in the following, we will be relying on models that predict the maximum number of photons, we are going to consider only the production due to proton primaries.

The composition of UHECR primaries will be much better known after AugerPrime [31,32] (see also [20] and references therein) operates for several years. This upgrade of Auger focuses on achieving mass–composition sensitivity for each extended air shower measured by its upgraded surface detector through multihybrid observations. If its planned resolution is achieved, AugerPrime should be able to distinguish between iron and proton primaries on an event-by-event basis at 90% C.L. and even separate iron from the CNO group at better than 50% CL. One of its design goals is to identify within five years of operation a proton fraction as low as 10% with 5σ statistical significance if such a component exists at the highest energies. AugerPrime is expected to be completed in 2023 and operate until at least 2032.

If it is confirmed that protons account for a certain fraction of the UHECRs, the level of UHECR photons will give an indication of the EGRB level, since these photons are absorbed in this background. In this paper, we show the upper limits on the EGRB that an observation of UHECR photons would imply, given a certain fraction of UHECR proton primaries.

The plan of the paper is the following. In Section 2, we explain how we model the sources and the propagation of particles. In Section 3, we present a revised version of our 2005 Figure 17 [28] showing the range of integrated GZK photon fluxes expected depending on the EGRB assumed. In Section 4, we show our results on the upper bounds

that an observation of UHECR photons could impose on the EGRB. In Section 5, we briefly conclude.

2. Diffuse GZK Photon Flux Calculation

To compute the flux of GZK photons produced by a homogeneous distribution of sources emitting originally only protons, we use a numerical code [33–35], which calculates the propagation of protons and photons using the kinematic equation approach and the standard dominant processes (see, e.g., [36]), which include photo-pion production by nucleons, e^+e^- pair production by protons, and neutron decay. The electromagnetic cascade simulation includes e^+e^- pair production by photons, inverse Compton scattering as well as two higher order processes, triplet pair production $e\gamma_b \rightarrow ee^+e^-$, and double pair production $\gamma\gamma_b \rightarrow e^+e^-e^+e^-$, where the background radiation photon γ_b spectrum is composed of the cosmic microwave background (CMB), radio, and IR/optic radiation. While the CMB and radio backgrounds strongly affect the GZK-photon flux, the IR/optic part of background radiation has and effect on the diffuse γ flux at TeV energies.

The calculation of the predicted GZK photon fluxes requires assumptions about the characteristics of the UHECR sources and backgrounds.

Potential sources that could emit protons and nuclei with energy above 10^{18} eV include gamma ray bursts, active galactic nuclei, and starbursts galaxies. We adopt some simplifying assumptions usually made about sources, namely that the UHECR emission rate is the same for all sources, that the spectrum and composition is independent of the redshift of the source, and that the emission rate is well described by a power-law spectrum. The parameterization of the initial proton flux that we use is

$$F(E) = f\,\frac{1}{E^{\alpha}}\,\exp\left(-\frac{E}{E_{\max}}\right). \tag{1}$$

The power law index α and maximum energy $E_{\max}$ are considered free parameters. We only consider $\alpha \geq 0$. The value $\alpha = 2.7$ roughly corresponds to the slope of the UHECR spectrum. Larger values of α disfavor having protons at higher energies. It is possible to adopt $\alpha = 0$ when considering the largest possible GZK photon fluxes (as we do in Section 4) if only the highest energy portion of cosmic ray spectrum consists of protons (see Figures 1 and 2).

The dependence of the GZK photon flux on the maximum energy $E_{\max}$ is more significant as α decreases. Since we are interested in favoring the production of GZK photons, here, we assume that $E_{\max} = 1 \times 10^{20}$ eV, a generous value considering that we assume a exponential cutoff (as opposed to a step function as we assumed in our earlier work [28]).

The amplitude f is fixed by requiring that the final proton differential spectrum from all sources does not exceed the observed UHECR spectrum, F_{CR}, which we assume to be that measured by TA [37]. To be more specific, we use the χ^2 criterion:

$$\begin{aligned} \chi^2_{upper}/N_{bins} &\equiv \sum_{F(E_i)>F_{CR}(E_i)} \frac{(F(E_i)-F_{CR}(E_i))^2}{\sigma^2_{CR}(E_i)} \leq 1, \text{ where} \\ N_{bins} &\equiv \sum_{F(E_i)>F_{CR}(E_i)} 1, \end{aligned} \tag{2}$$

where E_i is the ith bin middle energy, $F_{CR}(E_i)$ is the experimental cosmic flux, and $\sigma_{CR}(E_i)$ is its error in the ith bin. The sum is over bins for which the predicted spectrum is above the measured one. We choose the highest value of the amplitude f that satisfies the condition in Equation (2) (if allowed by the Fermi LAT [38] measurements of secondary gamma rays and the IceCube and Auger [39] upper bounds on secondary neutrinos, as explained below).

The UHECR spectrum has been measured by Auger [40] and TA [41]. A joint analysis showed that the TA spectrum is higher above the GZK cutoff [42]. We use it in this paper because it favors the production of GZK photons.

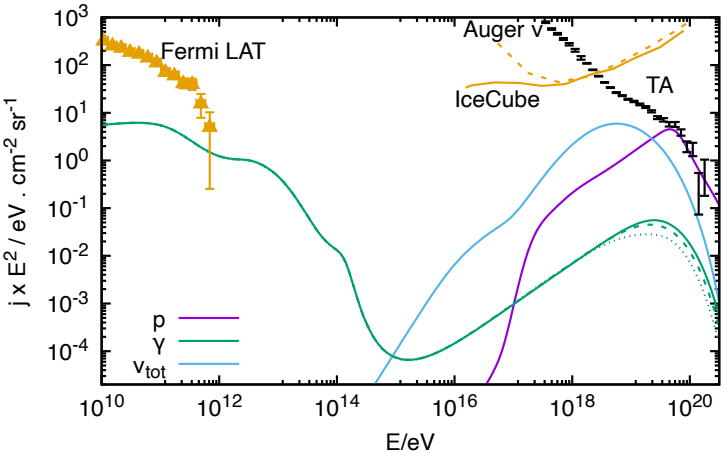

Figure 1. Example of the photon spectrum (green) produced by the the highest proton spectrum (magenta) normalized by the criterion in Equation (2) corresponding to the source model with $\alpha = 0$, $E_{\rm max} = 10^{20}$ eV, $m = 0$, $z_{\rm max} = 2$, and $z_{\rm min} = 0$. In this case, all UHECR flux above 40 EeV consists of protons. The green solid, dashed, and dotted UHECR photon lines correspond to 10% of the Clark et al. [43] EGRB and the higher and lower models of Protheroe and Biermann [44], respectively. The radio backgrounds were scaled down by the factor $F_{\rm rad} = 0.1$ because Figure 3 shows that this is the level for which the predicted UHECR photon flux could soon be observed, namely the level of current Auger upper limits. The isotropic diffuse photon flux measured by Fermi LAT [38] and the IceCube and Auger [39] upper bounds on all flavour neutrino diffuse flux, shown in ochre, are much higher than those predicted. This model predicts the highest level of GZK photons.

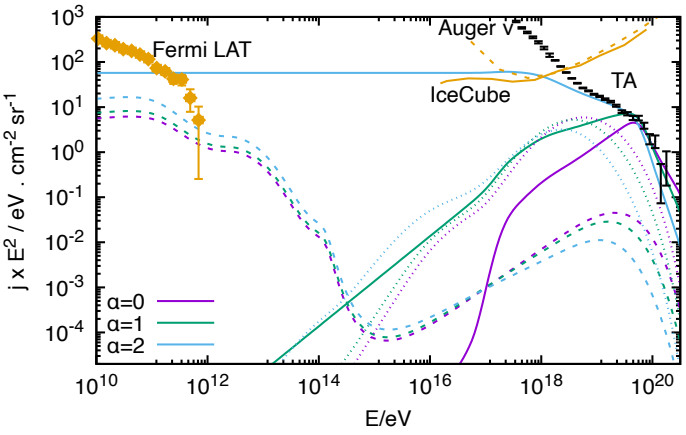

Figure 2. Highest primary proton spectrum allowed by the criterion in Equation (2) (solid lines), and secondary photon (dashed lines) and all flavor neutrino (doted lines) spectra produced in the model of Figure 1, but for different values power law index α ($\alpha = 0$, 1, and 2 in magenta, green, and sky blue, respectively). The lower radio background model of [44] is used, multiplied by $F_{\rm rad} = 0.1$ (as in Figure 1). The isotropic diffuse photon flux measured by Fermi LAT [38], shown in ochre, almost constrains the $\alpha = 2$ model as much as the limit in Equation (2) and is much above the predicted flux for the other two. The upper bounds on all flavor neutrino diffuse flux by IceCube and Auger [39], shown in ochre, do not constrain any of the models. The figure shows that the model of Figure 1 predicts the highest level of GZK photons.

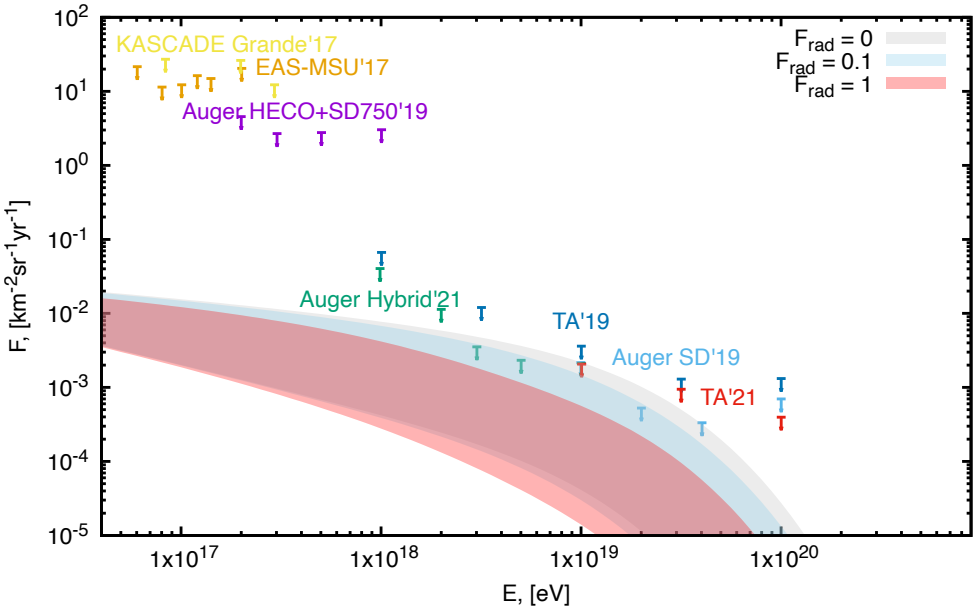

Figure 3. Bands of predicted UHECR photon fluxes assuming only proton primaries (whose maximum is at the level of the TA UHECR spectrum [37]) for source parameters $0 < \alpha < 2.8$, $-3 < m < 3$ and $E_{max} = 10^{20}$ eV and the injection spectrum in Equation (1). The bands in pink, sky blue, and gray assume respectively the lower radio background model of Protheroe and Biermann [44] multiplied by the factors $F_{\rm rad} = 1$, $F_{\rm rad} = 0.1$ and $F_{\rm rad} = 0$. Also shown are past and present experimental upper limits by Auger [26,27], TA [45,46], KASCADE Grande [47], and EAS-MSU [48].

The evolution of the density of the sources can be parameterized as

$$n(z) = n_0(1+z)^{3+m}\,\Theta(z_{\rm max}-z)\Theta(z-z_{\rm min})\,, \tag{3}$$

where m is a real parameter and $z_{\rm min}$ and $z_{\rm max}$ are respectively the redshifts of the closest and most distant sources. The source evolution in comoving volume is here parameterized by the index m, so that, excluding the Hubble expansion, the number density of sources is $\sim (1+z)^m$. In Section 4, we will assume that $m = 0$, which corresponds to nonevolving sources with constant density per comoving volume because as we show below (see Figure 4), GZK photons are produced closely enough such that their predicted flux is insensitive to the source evolution (see Figure 4). Since we are interested in estimating the maximum level of UHECR sources could produce, we assume that $z_{\rm min} = 0$, i.e., that the minimum distance to the sources is comparable to the interaction length. We take $z_{\rm max} = 2$, since sources with $z > 2$ have a negligible contribution to the UHECR flux above 10^{18} eV.

UHECR protons could interact with extragalactic magnetic fields (EGMF) during their propagation, but this effect is negligible for fields below 10^{-11} G (see Figure 5 of [28]), as found in constrained simulations. Numerical cosmological simulations give various predictions of the EGMF strength [49–54]. Lower limits on EGMFs can be found from combined observations of blazars by Fermi LAT and Cherenkov telescopes; depending on assumptions on source activity and other parameters, they can go up to $B > 10^{-15}$ G [55–57]. Upper limits at the 10^{-9} G level come from a variety of CMB observations (see Table 1 of [58]). More stringent upper limits of 10^{-10} G come from UHECR correlations with the Perseus-Pisces supercluster [59] and even 5×10^{-11} G from nonobservation of small-scale baryonic density fluctuations [58]. Here, we assume that EGMF are smaller than 10^{-11}G in the voids and neglect their influence on GZK photons.

Photons with energies $E_\gamma >$ TeV pair produce electrons and positrons on background photons, mostly CMB photons except at $E_\gamma > 10^{19}$ eV, initiating a cascade, which stops when the photons in it have $E_\gamma \simeq$ MeV to TeV. The flux of this extragalactic gamma ray background has been measured by Fermi-LAT [38] and is shown in Figure 1 (ochre points

with their error bars). The main extragalactic point sources contribution to the Fermi data at high energies are blazars. The contribution of unresolved blasars to the diffuse gamma-ray background dominates at high energies [60,61]. The Fermi collaboration determined that at least 86% of the EGRB comes from unresolved blazars [62], which strongly constrains UHECR models that predict high levels of GeV to TeV gamma rays, such as those with large positive values of the evolution index m.

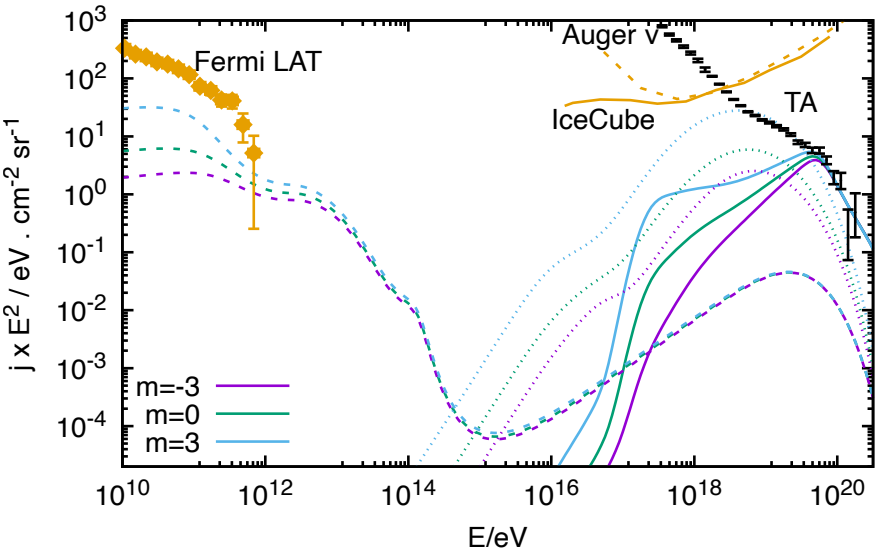

Figure 4. Highest primary proton spectrum allowed by the criterion in Equation (2) (solid lines), and corresponding photon (dashed lines) and all flavor neutrino (doted lines) spectra produced in the source model of Figure 1, but for different values of the source evolution parameter m ($m = -3$, 0, and 3 in magenta, green, and sky blue, respectively). The lower radio background model of [44] is used, multiplied by $F_{\rm rad} = 0.1$ (as in Figure 1). The isotropic diffuse photon flux measured by Fermi LAT [38] and the upper bounds on all flavor neutrino diffuse flux by IceCube and Auger [39], shown in ochre, do not constrain the primary proton flux. The figure shows that the predicted GZK photon spectrum is the same for all three evolution models.

The main source of energy loss of photons with $E_\gamma > 10^{19}$ eV is pair production on the radio background and the uncertainty in this background translates into uncertainty in the photon energy-attenuation length. As in our previous work [28–30], we consider three models for the EGRB: the background based on estimates by Clark et al. [43] and the two models of Protheroe and Biermann [44], both leading to a larger absorption of GZK photons than the first. The lowest model of Protheroe and Biermann has a level of about 0.1 of the ARCADE-2 [1] measurement.

Figure 1 shows examples of the GZK photon spectra (green lines) with a source model $\alpha = 0$, $E_{\rm max} = 1 \times 10^{20}$ eV, $z_{\rm max} = 2$, $z_{\rm min} = 0$, and evolution index $m = 0$ for three EGRB models with radio background scaled by a factor $F_{\rm rad} = 0.1$. The proton spectrum shown in magenta is the highest compatible with the condition in Equation (2). It provides a good fit to the TA spectrum above the GZK cutoff. Thus, it predicts a UHECR composition of only protons above the GZK cutoff.

The primary proton spectrum amplitude f for all models considered in this paper is determined as the largest allowed by the most constraining of three conditions (except in Section 4). One is the requirement in Equation (2) on the proton flux to avoid overproducing cosmic rays (for which we take the TA spectrum [37]) and conditions to avoid overproducing diffuse γ and ν fluxes. Another condition is based on the Fermi-LAT measurements of photons in the GeV to TeV energy range. Since at least 86% of these photons should come from unresolved BL Lac sources [62], we impose that the predicted integrated gamma ray flux above 50 GeV in the Fermi-LAT energy range should not exceed 0.14 times the

Fermi-LAT integrated spectrum above 50 GeV. The last condition on f is that the differential flux of secondary neutrinos of all types should not exceed the upper limits of IceCube and Auger [39]. For the models shown in Figures 1, 2 and 4, the last two conditions are never the most constraining.

The source model presented in Figure 1 is used in Section 4 as the most optimistic case in term of producing the highest levels of GZK photons, as proved in Figures 2 and 4. In Figure 4, the source model is the same as in Figure 1, but for different values of the source evolution parameter m, $m = -3$, 0, and 3. Figure 4 shows that the value of m has a negligible effect on GZK photon flux. Models with large enough positive values of m may in principle overproduce a diffuse γ flux in the sub-TeV energy range or a diffuse neutrino flux. The $m = 3$ scenario is almost equally constrained by the Fermi-LAT limit. The model with $m = 0$ is clearly safe with respect to diffuse γ and ν constraints while producing the same large GZK flux; therefore, we use it as baseline.

In Figure 2, we illustrate the dependence of the predicted GZK flux on the power law index α. The source model in this figure is the same as in Figure 1 except for the values of α. Figure 2 clearly shows that increasing α suppresses the GZK photon flux substantially, which dictates our use of $\alpha = 0$ in Section 4. The isotropic diffuse photon flux measured by Fermi-LAT [38] almost constrains the α =2 model as much as the limit in Equation (2) and is far above the predicted flux for $\alpha = 0$ and α =1.

The three EGRB models mentioned above result in the three different secondary photon spectra above 10^{18} eV shown in Figure 1. The green solid, dashed, and dotted UHECR photon lines correspond to 10% of the Clark et al. [43] model, 10% of the higher models, and 10% of the lower models of Protheroe and Biermann [44], respectively. The radio backgrounds were scaled down by 10%, i.e., by the factor $F_{\rm rad} = 0.1$, because Figure 3 shows that this is the radio background level for which the predicted UHECR photon flux could soon be observed, namely for which this predicted flux is at the level of current UHECR photon experimental upper limits.

3. Expected Range of the GZK Photon Flux

In this section, we update our 2005 results presented in Figure 17 [28] for the expected range of integrated GZK photon fluxes. In 2005, only extreme source models could predict fluxes at the level of the experimental UHECR photon upper limits. These limits have become much better now [26,27,45,46], as can be seen in Figure 3.

Figure 3 shows the band of UHECR photon predicted fluxes assuming only proton primaries (whose maximum is at the level of the TA UHECR spectrum [37]) for a range of source parameters assuming the injection spectrum in Equation (1): $0 < \alpha < 2.8$, $-3 < m < 3$ and, as throughout in this paper, $E_{\rm max} = 1 \times 10^{20}$ eV. The three bands in pink, sky blue, and gray assume respectively the lower radio background model of Protheroe and Biermann [44] ($F_{\rm rad} = 1$), 10% of it (i.e., the model mutiplied by the factor $F_{\rm rad} = 0.1$), and no radio background (i.e., $F_{\rm rad} = 0$).

The figure shows that the radio background level of 10% of the lower 1996 Protheroe and Biermann model leads to predicted photon fluxes at the level of the current photon upper limits. This EGRB level, 10% of the lower 1996 Protheroe and Biermann prediction, corresponds to 1% of the ARCADE-2 level [1] (a level predicted in some recent models [6,15]).

4. EGRB Upper Limit Expected from UHECR Photon Observation

The limits on UHECR photons have improved so much over the years, as shown in Figure 3, that reasonable although optimistic production models yield fluxes that could be detected in the near future. As mentioned in the introduction, much better measurements of the proton fraction of UHECR primaries is expected to be obtained after about five years of operation of AugerPrime.

Here, we compute the flux of UECR photons neglecting the production of photons by primaries other than protons, which is not correct for proton fractions close and below 0.1. We assume a reasonable but optimistic model that favors the production of photons,

the model of Figure 1, except for the amplitude f of the proton injection spectrum. With the maximum possible value of f this model fits well the UHECR spectrum above 40 EeV, with 100% proton primaries. Then, for each primary proton fraction, an observation of the UHECR photon flux would provide an upper limit on the EGRB, since a larger radio background would have suppressed the photon level to be below that observed. Namely if the radio background would be larger than the limit we find, even the maximum production model would lead to no signal.

For our optimistic production model we use the injection spectrum in Equation (1) with parameters $\alpha = 0$ and $E_{max} = 10^{20}$ eV, and the evolution parameters $m = 0$, $z_{\rm max} = 2$, $z_{\rm min} = 0$. This is the model of Figure 1. As discussed in Section 1, this choice leads to the largest GZK photon fluxes, and fits well the UHECR TA spectrum above 40EeV. Thus, in this model 100% of the UHECR consists of protons.

As it is clear from Figure 3, the most restrictive present limits on the GZK photon flux can be found in the energy range $18.5 < \log(E/eV) < 19.3$ (the exact energy depends on the value of $F_{\rm rad}$).

Let us assume that in the future the UHE photon flux is detected at the level $\eta \leq 1$ times the current limit at the most restrictive point. To obtain the minimal fraction of UHECR protons needed to generate enough GZK photons if $\eta = 1$, we divide each present integrated photon flux limit by the predicted photon flux, computed assuming a 100% UHECR proton primary composition above 4×10^{19} eV and a particular level of the radio background. Then, we find the minimum value of this ratio among all the present limits. This minimum ratio determines the minimum fraction of protons in the UHECRs above 4×10^{19} eV required to produce the photon signal. Clearly, since we consider only photon production from primary protons, for other values of η the required minimal proton fraction scales linearly with η. The constraints obtained in this way for different values of the EGRB scale factor $F_{\rm rad}$ are shown in Figure 5. Since we are assuming that the fraction of proton primaries will be measured by AugerPrime, we reverse the constraints and show limits on $F_{\rm rad}$.

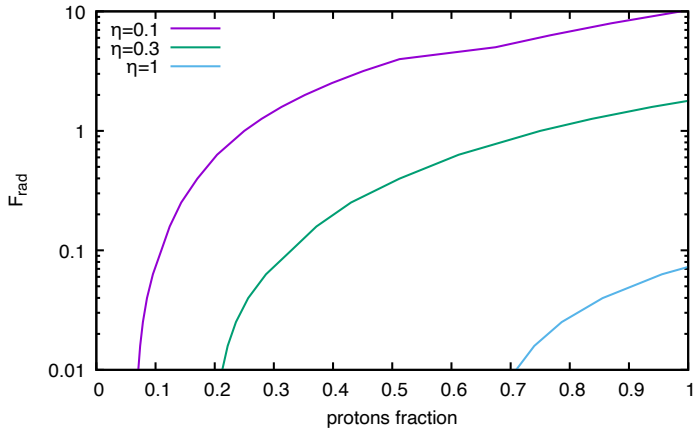

Figure 5. Upper limit on the EGRB, given as a factor $F_{\rm rad}$ times the lower radio background prediction of Protheroe and Biermann [44], which could be achieved if a GZK photon flux is detected at a level $\eta = 0.1$ (magenta), $\eta = 0.3$ (green), and $\eta = 1$ (blue) of the present Auger UHECR photon limits [26,27], shown as function of the proton fraction in UHECRs (to be determined in the future by AugerPrime). The limits for other η values can be easily obtained since they scale linearly with η. The production of photons from primaries other than protons is neglected here (which would not be consistent with small proton fractions, close and below 0.1). The source model parameters assumed are $\alpha = 0$, $E_{max} = 10^{20}$ eV, $m = 0$, $z_{max} = 2$, $z_{min} = 0$. $F_{\rm rad} = 10$ corresponds to the ARCADE-2 measurement [1]. Notice that for a particular value of $F_{\rm rad}$, the corresponding proton fraction for a particular η is the minimum proton fraction compatible with the photon observation at the level indicated by η.

In Figure 5 the upper limits on the EGRB are shown as function of the UHECR proton fraction above 4×10^{19} eV to be determined by AugerPrime, in terms of the factor $F_{\rm rad}$ by which the lower radio background prediction of Protheroe and Biermann [44] should be multiplied, assuming an observation of UHECR photons at the level of the present limits or smaller by a factor η. Only lines for $\eta = 0.1$ (magenta), $\eta = 0.3$ (green), and $\eta = 1$ (blue) are shown; however, the lines scale linearly with the fraction η, so the line for any other η value can be easily obtained. Notice that $F_{\rm rad} = 10$ corresponds to the ARCADE-2 measurement [1].

As a final comment, let us mention that potentially a lower limit on the EGRB could be established if the UHECR proton primary content is proved to be high enough and GZK photons are not observed. Deriving this limit would require to take into account the observed spectrum and directional information of the proton primaries. This type of analysis is beyond the scope of this paper.

5. Conclusions

In this paper, we studied the possibility of deriving an upper limit on the diffuse extragalactic radio background from a possible future detection of the GZK photon flux. Our main result is summarized in Figure 5. Assuming the photon flux observed is at a level of the factor η times the current upper limits on UHECR photons, and given a particular proton fraction in the UHECRs above 40 EeV, one can establish an upper limit on the diffuse radio background. For example, for a photon flux three times lower than the present limits, i.e., with $\eta = 0.3$, and a proton fraction 0.5 (which is consistent with current TA data), one can exclude a radio background above the lower radio background prediction of Protheroe and Biermann [44].

Author Contributions: Conceptualization, methodology, validation, formal analysis, investigation, resources, writing—original draft preparation, writing—review and editing, project administration, funding acquisition, G.B.G., O.K. and D.S.; software, data curation, visualization, O.K. All authors have read and agreed to the published version of the manuscript.

Funding: The work of GBG was supported in part by the U.S. Department of Energy (DOE) Grant No. DE-SC0009937. Work of O.K. is supported in the framework of the State project "Science" by the Ministry of Science and Higher Education of the Russian Federation under the contract 075-15-2020-778.

Acknowledgments: We thank Peter L. Biermann for several clarifying discussions about radio background observations and models.

Conflicts of Interest: The funders had no role in the design of the study; in the collection, analyses, or interpretation of data; in the writing of the manuscript, or in the decision to publish the results.

References

1. Fixsen, D.J.; Kogut, A.; Levin, S.; Limon, M.; Lubin, P.; Mirel, P.; Seiffert, M.; Singal, J.; Wollack, E.; Villela, T.; et al. ARCADE 2 Measurement of the Extra-Galactic Sky Temperature at 3–90 GHz. *Astrophys. J.* **2011**, *734*, 5. [CrossRef]
2. Dowell, J.; Taylor, G.B. The Radio Background Below 100 MHz. *Astrophys. J. Lett.* **2018**, *858*, L9. [CrossRef]
3. Singal, J.; Haider, J.; Ajello, M.; Ballantyne, D.R.; Bunn, E.; Condon, J.; Dowell, J.; Fixsen, D.; Fornengo, N.; Harms, B.; et al. The Radio Synchrotron Background: Conference Summary and Report. *Publ. Astron. Soc. Pac.* **2018**, *130*, 036001. [CrossRef]
4. Fraser, S.; Hektor, A.; Hutsi, G.; Kannike, K.; Marzo, C.; Marzola, L.; Spethmann, C.; Racioppi, A.; Raidal, M.; Vaskonen, V.; et al. The EDGES 21 cm Anomaly and Properties of Dark Matter. *Phys. Lett. B* **2018**, *785*, 159–164. [CrossRef]
5. Pospelov, M.; Pradler, J.; Ruderman, J.T.; Urbano, A. Room for New Physics in the Rayleigh-Jeans Tail of the Cosmic Microwave Background. *Phys. Rev. Lett.* **2018**, *121*, 031103. [CrossRef]
6. Jana, R.; Nath, B.B.; Biermann, P.L. Radio background and IGM heating due to Pop III supernova explosions. *Mon. Not. Roy. Astron. Soc.* **2019**, *483*, 5329–5333. [CrossRef]
7. Brandenberger, R.; Cyr, B.; Shi, R. Constraints on Superconducting Cosmic Strings from the Global 21-cm Signal before Reionization. *J. Cosmol. Astropart. Phys.* **2019**, *2019*, 009. [CrossRef]
8. Chianese, M.; Di Bari, P.; Farrag, K.; Samanta, R. Probing relic neutrino radiative decays with 21 cm cosmology. *Phys. Lett. B* **2019**, *790*, 64–70. [CrossRef]

9. Lawson, K.; Zhitnitsky, A.R. The 21 cm absorption line and the axion quark nugget dark matter model. *Phys. Dark Univ.* **2019**, *24*, 100295. [CrossRef]
10. Ewall-Wice, A.; Chang, T.C.; Lazio, J.; Dore, O.; Seiffert, M.; Monsalve, R.A. Modeling the Radio Background from the First Black Holes at Cosmic Dawn: Implications for the 21 cm Absorption Amplitude. *Astrophys. J.* **2018**, *868*, 63. [CrossRef]
11. Ewall-Wice, A.; Chang, T.C.; Lazio, T.J.W. The Radio Scream from black holes at Cosmic Dawn: A semi-analytic model for the impact of radio-loud black holes on the 21 cm global signal. *Mon. Not. Roy. Astron. Soc.* **2020**, *492*, 6086–6104. [CrossRef]
12. Mittal, S.; Kulkarni, G. Background of radio photons from primordial black holes. *Mon. Not. Roy. Astron. Soc.* **2022**, *510*, 4992–4997. [CrossRef]
13. Krause, M.G.H.; Hardcastle, M.J. Can the Local Bubble explain the radio background? *Mon. Not. Roy. Astron. Soc.* **2021**, *502*, 2807–2814. [CrossRef]
14. Bowman, J.D.; Rogers, A.E.E.; Monsalve, R.A.; Mozdzen, T.J.; Mahesh, N. An absorption profile centred at 78 megahertz in the sky-averaged spectrum. *Nature* **2018**, *555*, 67–70. [CrossRef] [PubMed]
15. Feng, C.; Holder, G. Enhanced global signal of neutral hydrogen due to excess radiation at cosmic dawn. *Astrophys. J. Lett.* **2018**, *858*, L17. [CrossRef]
16. Kachelriess, M.; Semikoz, D.V. Cosmic Ray Models. *Prog. Part. Nucl. Phys.* **2019**, *109*, 103710, [CrossRef]
17. Greisen, K. End to the cosmic ray spectrum? *Phys. Rev. Lett.* **1966**, *16*, 748–750. [CrossRef]
18. Zatsepin, G.T.; Kuzmin, V.A. Upper limit of the spectrum of cosmic rays. *JETP Lett.* **1966**, *4*, 78–80.
19. Kuznetsov, M.Y.; Tinyakov, P.G. UHECR mass composition at highest energies from anisotropy of their arrival directions. *J. Cosmol. Astropart. Phys.* **2021**, *2021*, 065. [CrossRef]
20. Coleman, A.; Eser, J.; Mayotte, E.; Sarazin, F.; Schröder, F.G.; Soldin, D.; Venters, T.M.; Aloisio, R.; Alvarez-Muniz, J.; Alves Batista, R.; et al. Ultra-High-Energy Cosmic Rays: The Intersection of the Cosmic and Energy Frontiers. *arXiv* **2022**, arXiv:2205.05845.
21. Bergman, D. Telescope Array Combined Fit to Cosmic Ray Spectrum and Composition. *PoS* **2021**, *ICRC2021*, 338. [CrossRef]
22. Aab, A.; et al. [Pierre Auger Collaboration] Inferences on mass composition and tests of hadronic interactions from 0.3 to 100 EeV using the water-Cherenkov detectors of the Pierre Auger Observatory. *Phys. Rev. D* **2017**, *96*, 122003. [CrossRef]
23. Abbasi, R.U.; et al. [Telescope Array Collaboration] Mass composition of ultrahigh-energy cosmic rays with the Telescope Array Surface Detector data. *Phys. Rev. D* **2019**, *99*, 022002. [CrossRef]
24. Abraham, J.; Aglietta, M.; Aguirre, C.; Allard, D.; Allekotte, I.; Allison, P.; Alvarez, C.; Alvarez-Muniz, J.; Ambrosio, M.; Anchordoqui, L.; et al. An upper limit to the photon fraction in cosmic rays above 10^{19}-eV from the Pierre Auger Observatory. *Astropart. Phys.* **2007**, *27*, 155–168. [CrossRef]
25. Abbasi, R.U.; et al. [Telescope Array Collaboration] Search for point sources of ultra-high-energy photons with the Telescope Array surface detector. *Mon. Not. Roy. Astron. Soc.* **2020**, *492*, 3984–3993. [CrossRef]
26. Savina, P.; et al. [The Pierre Auger Collaboration] A search for ultra-high-energy photons at the Pierre Auger Observatory exploiting air-shower universality. *PoS* **2021**, *ICRC2021*, 373. [CrossRef]
27. Rautenberg, J. Limits on ultra-high energy photons with the Pierre Auger Observatory. *PoS* **2021**, *ICRC2019*, 398. [CrossRef]
28. Gelmini, G.; Kalashev, O.E.; Semikoz, D.V. GZK photons as ultra high energy cosmic rays. *J. Exp. Theor. Phys.* **2008**, *106*, 1061–1082. [CrossRef]
29. Gelmini, G.; Kalashev, O.E.; Semikoz, D.V. GZK Photons in the Minimal Ultrahigh Energy Cosmic Rays Model. *Astropart. Phys.* **2007**, *28*, 390–396. [CrossRef]
30. Gelmini, G.B.; Kalashev, O.E.; Semikoz, D.V. GZK Photons Above 10-EeV. *J. Cosmol. Astropart. Phys.* **2007**, *2007*, 002. [CrossRef]
31. Aab, A.; et al. [The Pierre Auger Collaboration] The Pierre Auger Observatory Upgrade-Preliminary Design Report. *arXiv* **2016**, arXiv:1604.03637.
32. Castellina, A. AugerPrime: The Pierre Auger Observatory Upgrade. *EPJ Web Conf.* **2019**, *210*, 06002. [CrossRef]
33. Kalashev, O.E.; Kuzmin, V.A.; Semikoz, D.V. Top down models and extremely high-energy cosmic rays. *arXiv* **1999**, arXiv:astro-ph/9911035.
34. Kalashev, O.E.; Kuzmin, V.A.; Semikoz, D.V. Ultrahigh-energy cosmic rays. Propagation in the galaxy and anisotropy. *Mod. Phys. Lett. A* **2001**, *16*, 2505–2515. [CrossRef]
35. Kalashev, O.E.; Kido, E. Simulations of Ultra High Energy Cosmic Rays propagation. *J. Exp. Theor. Phys.* **2015**, *120*, 790–797. [CrossRef]
36. Bhattacharjee, P.; Sigl, G. Origin and propagation of extremely high-energy cosmic rays. *Phys. Rept.* **2000**, *327*, 109–247. [CrossRef]
37. Ivanov, D. Energy Spectrum Measured by the Telescope Array. *PoS* **2020**, *ICRC2019*, 298. [CrossRef]
38. Ackermann, M.; Ajello, M.; Albert, A.; Atwood, W.B.; Baldini, L.; Ballet, J.; Barbiellini, G.; Bastieri, D.; Bechtol, K.; Bellazzini, R.; et al. The spectrum of isotropic diffuse gamma-ray emission between 100 MeV and 820 GeV. *Astrophys. J.* **2015**, *799*, 86. [CrossRef]
39. Parente, G. The Search for Ultra-High Energy Neutrinos through Highly Inclined Air Showers in the Pierre Auger Observatory. *J. Phys. Conf. Ser.* **2021**, *2156*, 012095. [CrossRef]
40. Aab, A.; et al. [The Pierre Auger Collaboration] Measurement of the cosmic-ray energy spectrum above 2.5×10^{18} eV using the Pierre Auger Observatory. *Phys. Rev. D* **2020**, *102*, 062005. [CrossRef]
41. Ivanov, D.; Bergman, D.; Furlich, G.; Gonzalez, R.; Thomson, G.; Tsunesada, Y. Recent measurement of the Telescope Array energy spectrum and observation of the shoulder feature in the Northern Hemisphere. *PoS* **2021**, *ICRC2021*, 341. [CrossRef]

42. Tsunesada, Y.; Abbasi, R.; Abu-Zayyad, T.; Allen, M.; Arai, Y.; Arimura, R.; Barcikowski, E.; Belz, J.; Bergman, D.; Blake, S.; et al. Joint analysis of the energy spectrum of ultra-high-energy cosmic rays as measured at the Pierre Auger Observatory and the Telescope Array. *PoS* **2021**, *ICRC2021*, 337. [CrossRef]
43. Clark, T.A.; Brown, L.W.; Alexander, J.K. Spectrum of the Extra-galactic Background Radiation at Low Radio Frequencies. *Nature* **1970**, *228*, 847–849. [CrossRef]
44. Protheroe, R.J.; Biermann, P.L. A New estimate of the extragalactic radio background and implications for ultrahigh-energy gamma-ray propagation. *Astropart. Phys.* **1996**, *6*, 45–54. Erratum in *Astropart. Phys.* **1997**, *7*, 181. [CrossRef]
45. Abbasi, R.U.; Abe, M.; Abu-Zayyad, T.; Allen, M.; Arimura, R.; Barcikowski, E.; Belz, J.W.; Bergman, D.R.; Blake, S.A.; Cady, R.; et al. Constraints on the diffuse photon flux with energies above 10^{18} eV using the surface detector of the Telescope Array experiment. *Astropart. Phys.* **2019**, *110*, 8–14. [CrossRef]
46. Kalashev, O.E.; et al. [Telescope Array Collaboration] Telescope Array search for EeV photons. *PoS* **2021**, *ICRC2021*, 864. [CrossRef]
47. Apel, W.D.; Arteaga-Velázquez, J.C.; Bekk, K.; Bertaina, M.; Blümer, J.; Bozdog, H.; Brancus, I.M.; Cantoni, E.; Chiavassa, A.; Cossavella, F.; et al. KASCADE-Grande Limits on the Isotropic Diffuse Gamma-Ray Flux between 100 TeV and 1 EeV. *Astrophys. J.* **2017**, *848*, 1. [CrossRef]
48. Fomin, Y.A.; Kalmykov, N.N.; Karpikov, I.S.; Kulikov, G.V.; Kuznetsov, M.Y.; Rubtsov, G.I.; Sulakov, V.P.; Troitsky, S.V. Constraints on the flux of $\sim (10^{16} - 10^{17.5})$ eV cosmic photons from the EAS-MSU muon data. *Phys. Rev. D* **2017**, *95*, 123011. [CrossRef]
49. Garcia, A.A.; Bondarenko, K.; Boyarsky, A.; Nelson, D.; Pillepich, A.; Sokolenko, A. Ultra-high energy cosmic rays deflection by the Intergalactic Magnetic Field. *arXiv* **2021**, arXiv:2101.07207.
50. Sigl, G.; Miniati, F.; Ensslin, T.A. Ultrahigh energy cosmic ray probes of large scale structure and magnetic fields. *Phys. Rev. D* **2004**, *70*, 043007. [CrossRef]
51. Dolag, K.; Grasso, D.; Springel, V.; Tkachev, I. Constrained simulations of the magnetic field in the local Universe and the propagation of UHECRs. *J. Cosmol. Astropart. Phys.* **2005**, *2005*, 009. [CrossRef]
52. Hackstein, S.; Vazza, F.; Brüggen, M.; Sigl, G.; Dundovic, A. Propagation of ultrahigh energy cosmic rays in extragalactic magnetic fields: A view from cosmological simulations. *Mon. Not. Roy. Astron. Soc.* **2016**, *462*, 3660–3671. [CrossRef]
53. Hackstein, S.; Vazza, F.; Brüggen, M.; Sorce, J.G.; Gottlöber, S. Simulations of ultra-high Energy Cosmic Rays in the local Universe and the origin of Cosmic Magnetic Fields. *Mon. Not. Roy. Astron. Soc.* **2018**, *475*, 2519–2529. [CrossRef]
54. Alves Batista, R.; Shin, M.S.; Devriendt, J.; Semikoz, D.; Sigl, G. Implications of strong intergalactic magnetic fields for ultrahigh-energy cosmic-ray astronomy. *Phys. Rev. D* **2017**, *96*, 023010. [CrossRef]
55. Neronov, A.; Vovk, I. Evidence for Strong Extragalactic Magnetic Fields from Fermi Observations of TeV Blazars. *Science* **2010**, *328*, 73–75. [CrossRef] [PubMed]
56. Taylor, A.M.; Vovk, I.; Neronov, A. Extragalactic magnetic fields constraints from simultaneous GeV–TeV observations of blazars. *Astron. Astrophys.* **2011**, *529*, A144. [CrossRef]
57. Ackermann, M.; Ajello, M.; Baldini, L.; Ballet, J.; Barbiellini, G.; Bastieri, D.; Bellazzini, R.; Bissaldi, E.; Blandford, R.D.; Bloom, E.D.; et al. The Search for Spatial Extension in High-latitude Sources Detected by the *Fermi* Large Area Telescope. *Astrophys. J. Suppl.* **2018**, *237*, 32. [CrossRef]
58. Jedamzik, K.; Saveliev, A. Stringent Limit on Primordial Magnetic Fields from the Cosmic Microwave Background Radiation. *Phys. Rev. Lett.* **2019**, *123*, 021301. [CrossRef]
59. Neronov, A.; Semikoz, D.; Kalashev, O. Limit on intergalactic magnetic field from ultra-high-energy cosmic ray hotspot in Perseus-Pisces region. *arXiv* **2021**, arXiv:2112.08202.
60. Neronov, A.; Semikoz, D.V. Extragalactic Very-High-Energy gamma-ray background. *Astrophys. J.* **2012**, *757*, 61. [CrossRef]
61. Di Mauro, M.; Donato, F.; Lamanna, G.; Sanchez, D.A.; Serpico, P.D. Diffuse γ-ray emission from unresolved BL Lac objects. *Astrophys. J.* **2014**, *786*, 129. [CrossRef]
62. Ackermann, M.; Ajello, M.; Albert, A.; Atwood, W.B.; Baldini, L.; Ballet, J.; Barbiellini, G.; Bastieri, D.; Bechtol, K.; Bellazzini, R.; et al. Resolving the Extragalactic γ-Ray Background above 50 GeV with the Fermi Large Area Telescope. *Phys. Rev. Lett.* **2016**, *116*, 151105. [CrossRef] [PubMed]